

# $gg \rightarrow ZH$ at NLO matched to parton showers with ggxy and POWHEG

---

Joshua Davies,<sup>a</sup> Kay Schönwald,<sup>b</sup> Matthias Steinhauser,<sup>c</sup> Daniel Stremmer<sup>c</sup>

<sup>a</sup>*Department of Mathematical Sciences, University of Liverpool, Liverpool, L69 3BX, UK*

<sup>b</sup>*Theoretical Physics Department, CERN, 1211 Geneva 23, Switzerland*

<sup>c</sup>*Institut für Theoretische Teilchenphysik, Karlsruhe Institute of Technology (KIT), Wolfgang-Gaede Straße 1, 76131 Karlsruhe, Germany*

*E-mail:* [J.O.Davies@liverpool.ac.uk](mailto:J.O.Davies@liverpool.ac.uk), [kay.schonwald@cern.ch](mailto:kay.schonwald@cern.ch),  
[matthias.steinhauser@kit.edu](mailto:matthias.steinhauser@kit.edu), [daniel.stremmer@kit.edu](mailto:daniel.stremmer@kit.edu)

ABSTRACT:

We implement the recently-calculated analytic expressions for the next-to-leading order QCD corrections to  $gg \rightarrow ZH$  in ggxy. This provides a flexible framework for investigating partonic and hadronic cross sections for various top quark mass renormalization schemes. We augment the  $Z$  boson with leptonic decays, including spin correlations and off-shell effects, and furthermore provide an interface to POWHEG. This enables simulations with parton showers, performed using Pythia.

---

## Contents

<b>1</b>	<b>Introduction</b>	<b>2</b>
<b>2</b>	<b>Implementing <math>gg \rightarrow ZH</math> to NLO QCD in ggxy</b>	<b>3</b>
<b>3</b>	<b>Hadronic fixed-order cross sections with ggxy</b>	<b>8</b>
3.1	Stable $Z$ bosons	8
3.2	Off-shell $Z$ bosons and leptonic decays	9
3.3	Combination with <code>vh@nnlo</code>	12
<b>4</b>	<b><math>gg \rightarrow ZH</math> at NLO matched to a parton shower</b>	<b>14</b>
4.1	Implementation in POWHEG: <code>ggxy_ggZH</code>	14
4.2	Cross checks with ggxy	15
4.3	Numerical results for parton showers with Pythia	16
<b>5</b>	<b>Conclusions</b>	<b>19</b>

---

# 1 Introduction

The associated production of a Higgs boson with a gauge boson is an important process for investigating the properties of the Higgs boson. The experimental precision obtained at the Large Hadron Collider (LHC) is steadily increasing (see, e.g., Refs. [1, 2]) which demands the continuous increase in precision of theory predictions.

Whereas the associated  $WH$  production is only possible through a Drell-Yan type process, for  $ZH$  production there is in addition a gluon-induced channel, which is numerically important. In recent years many higher-order corrections have been computed both for the total cross section and for differential distributions [3–15] including the resummation of soft gluon effects [16–18]. Most of them are implemented in the publicly available computer codes `vh@nnlo` [19, 20] and `HAWK` [21, 22]. In this work we concentrate on the process  $gg \rightarrow ZH$  and implement it in the library `ggxy` [23] including next-to-leading order (NLO) QCD corrections which are, to date, not available in public computer codes. `ggxy` is written in C++, and due to its modular structure it provides a fast and flexible framework to compute partonic and hadronic cross sections. It is possible to choose either the pole or the  $\overline{\text{MS}}$  scheme for the top quark mass. The implementation closely follows that of  $gg \rightarrow HH$  at NLO QCD, which is described in Ref. [23].

The results discussed in this paper are based on the analytic expressions obtained in the large top quark mass limit [15], around the forward limit, and for high energies [14]. In Section 2 we describe the implementation in `ggxy` [23] and report on the validation against known results. We also describe the implementation of leptonic  $Z$  boson decays, including off-shell effects and spin correlations. In Section 3 we show how hadronic cross sections are computed for both stable and decaying  $Z$  bosons. Example files show how `ggxy` can be used to reproduce results from the literature available for stable  $Z$  bosons. For stable  $Z$  bosons we can combine our results with the Drell-Yan contributions from `vh@nnlo`, which is also discussed in Section 3.

Section 4 is dedicated to the interface of `ggxy` to `POWHEG`, again with the option for stable or unstable  $Z$  bosons. We validate against `ggxy` and then move on to simulations including parton showers with `PYTHIA` [24]. Note that within the `POWHEG` framework the Higgs boson is stable (though may be off-shell). Higgs boson decays can be performed together with the parton showers. We conclude in Section 5.

The example files shipped together with `ggxy` should allow anyone to implement the process  $gg \rightarrow ZH$ , including NLO QCD corrections, into their own analysis code.

The `ggxy` library can be downloaded from <https://gitlab.com/ggxy/ggxy-release>. For the installation of `ggxy` we refer to Section 4 of the original paper [23]. Since the analytic expressions for the various expansions are quite large, compilation time is approximately an hour. It can be reduced by selecting only the required processes (`ggHH` or `ggZH`) in the file `example-build.sh`.

## 2 Implementing $gg \rightarrow ZH$ to NLO QCD in `ggxy`

For our calculation and implementation in `ggxy` we consider the two-loop amplitudes, required for the NLO QCD corrections, that have been calculated in Ref. [14] using two complementary expansion methods; the forward and high-energy expansions. In the forward expansion we consider a hierarchy in which the Mandelstam variable  $t$  and the external virtualities<sup>1</sup>  $q_Z^2$  and  $q_H^2$  are the smallest scales of this process:  $|t|, q_Z^2, q_H^2 \ll m_t^2, s$ . In the high-energy expansion we consider  $q_Z^2, q_H^2 \ll m_t^2 \ll s, |t|$ . In particular, it was also shown in Ref. [14] that these two expansions methods cover the full phase space with high precision.

The amplitude for  $gg \rightarrow ZH$  is expressed in terms of six independent form factors,

$$F_{12}^+(t, u), F_{12}^-(t, u), F_2^-(t, u), F_3^+(t, u), F_3^-(t, u), F_4(t, u), \quad (2.1)$$

see also Eqs. (34) and (36) of Ref. [14] for more details. We have implemented the analytic expressions of the two expansion methods for all form factors, and provide functions which automatically use the appropriate expansion following a similar logic as for  $gg \rightarrow HH$ , which is described in detail in Ref. [23]. For  $gg \rightarrow ZH$  there are a few differences which we describe in the following. First, we use different switching points between the two expansions for different form factors, which range from  $200 \text{ GeV} < p_T < 260 \text{ GeV}$  for any value of  $\sqrt{s}$ . In addition, we construct Padé approximations following Ref. [25] not only for the high-energy but also for the forward expansions if  $p_T > 180 \text{ GeV}$ . This improves the convergence of the series such that both expansions have a similar accuracy at the switching points. In order to improve the numerical stability of the high-energy expansion we perform an additional expansion in  $-t/s$  if this ratio is smaller than 0.05. For small center-of-mass energies below  $\sqrt{s} < 200 \text{ GeV}$  we switch from the forward expansion to the large top-quark mass expansion to improve the numerical stability and evaluation time. The latter expansion has been implemented in `ggxy` up to three loops in Ref. [15]. We note that at LO we use the exact expressions that have been implemented in combination with `OneL0op` [26] for the evaluation of the one-loop scalar integrals and for the double triangle contribution we use the expressions from Ref. [9].

The core of the implementation consists of the six form factors in Eq. (2.1) at one- and two-loop order from which the (partonic) Born cross section and virtual corrections used for the hadronic cross sections are computed. In the following we present the prototypes of the `C++` functions, which defines the input and output values in a unique way. The one- and two-loop form factors can be computed with

```
complex<double> ggzhFF(int loops, string/int ff, double s, double t,
    double mzs, double mhs, double mts,
    double murs = ggzhFFmursDefault,
    double muts = 0.0, unsigned scheme = 0,
    complex<double> kappa_hzz = 1.0,
    double dTriCoeff = 1.0),
```

---

<sup>1</sup>Note that both the Higgs boson and  $Z$  boson can be off-shell.

where the input parameters are defined as,

- loops:** QCD loop order, 1 or 2
- ff:** choice of form factor, either as a string "F12p", "F12m", "F2m", "F3p", "F3m", "F4" or as an integer between 1,...,6 following the same ordering
- s, t:** Mandelstam variables
- mzs:** squared Z boson mass,  $m_Z^2$ , can be off-shell
- mhs:** squared Higgs boson mass,  $m_H^2$ , can be off-shell
- mts:** squared top quark mass,  $m_t^2$
- murs:** squared renormalization scale  $\mu_r^2$
- mut:** squared renormalization scale for the  $\overline{\text{MS}}$  top quark mass  $\mu_t^2$
- scheme:** choice of renormalization scheme for top quark mass, 0 (OS) or 1 ( $\overline{\text{MS}}$ ).
- kappa\_hzz:** corresponds to  $\kappa_{HZZ}$  which multiplies the  $HZZ$  vertex.  $\kappa_{HZZ} = 1$  corresponds to the Standard Model value
- dTriCoeff:** additional coefficient for the double-triangle contribution, can, e.g., be used to switch on and off the double-triangle contribution

The default value of the squared renormalization scale, **murs**, is set to the pre-processor variable **ggzhFFmursDefault** which is a placeholder for  $\mu_r^2 = -s$ . In addition there are also low-level functions which implement the forward and high-energy expansions of the form factors. They are also accessible to the user, however we refrain from describing them in detail since they are not used directly in this paper.

The (finite) virtual corrections are implemented as  $\mathcal{V}_{\text{fin}}$  (see Eqs. (38) and (39) of Ref. [14] for an explicit formula). The C++ implementation can be called with

```
double ggzh2lvfin(double s, double t, double mzs, double mhs, double mts,
                 double GF, double murs = ggzhFFmursDefault,
                 double muts = 0.0, unsigned scheme = 0,
                 double kappa_hzz = 1.0, double dTriCoeff = 1.0);
```

where the input parameters are the same as before and additionally **GF** stands for the Fermi constant  $G_F$ . Note that in contrast to **ggzhFF**, here and in the following the masses  $m_Z$  and  $m_H$  have to be on-shell. In addition, the pre-processor variable **ggzhFFmursDefault** is, in this case, a placeholder for  $\mu_r^2 = s/4$ . Alternatively, the function

```
vector<double> ggzh2l(double s, double t, double mzs, double mhs,
                    double mts, double GF,
                    double murs = ggzhFFmursDefault,
                    double muts = 0.0, unsigned scheme = 0,
                    double kappa_hzz = 1.0, double dTriCoeff = 1.0);
```

can be used which returns a vector with the LO squared matrix element as the first and  $\mathcal{V}_{\text{fin}}$  as the second element. The one-loop squared matrix elements can also be computed with

```
double ggzh1l(double s, double t, double mzs, double mhs, double mts,
              double GF, double kappa_hzz = 1.0);
```

For the computation of the hadronic cross sections we use the generic code developed for  $gg \rightarrow HH$  [23]. We will provide more details in Section 3 where several examples are discussed in detail.

The implementation of the real corrections also closely follow our approach for  $gg \rightarrow HH$ . We use the Catani-Seymour subtraction scheme [27] and the  $2 \rightarrow 3$  matrix elements are calculated with `Recola` [28, 29] in combination with `Collier` [30]. In addition, we use an alternative reduction to scalar integrals using the OPP reduction technique [31] implemented in `CutTools` [32], for phase-space points that are marked by `Collier` to contain possibly unstable tensor integrals. In this approach the scalar integrals are calculated with `OneLOop` [26].

The real corrections consist of the following sub-processes:

$$\begin{aligned}
 gg &\rightarrow ZHg, & qq/qg &\rightarrow ZHq, \\
 q\bar{q}/\bar{q}q &\rightarrow ZHg, & g\bar{q}/\bar{q}g &\rightarrow ZH\bar{q}.
 \end{aligned}
 \tag{2.2}$$

Special care has to be taken for quark-initiated sub-processes, as they contain also contributions from Higgs-Strahlung type diagrams. For the calculation of NLO QCD corrections to  $gg \rightarrow ZH$  we discard all such contributions (see Fig. 1(a)) and take into account only contributions with a single closed quark loop. The latter can be divided into two classes: Either both the  $Z$  and the Higgs bosons are attached to the closed quark loop, or only the Higgs boson is attached to the closed quark loop while the  $Z$  is radiated from an external quark line, see Fig. 1(b)-(e). The second class of diagrams forms a gauge-invariant and finite subset and was not included in the calculation of Ref. [13], while in Refs. [33, 34] both classes were considered. Note that the second class has only a minor impact at the integrated level, however it can significantly impact the high-energy region of the distributions.

Since `Recola` does not work with Feynman diagrams but instead generates amplitudes using the recursive approach of Ref. [35], the filtering of Higgs-Strahlung type diagrams and the separation of the two classes is not straightforward. However, we managed to eliminate the Drell-Yan-type diagrams and to implement in `Recola` the possibility to obtain either only the contribution from diagrams where the  $Z$  boson is attached to a closed fermion loop, or both classes of diagrams together. Our implementation has been cross-checked for single phase-space points with reference values from Ref. [34]. In `ggxy` this option is implemented with the switch `iopt_ext_Z`, see the examples below for more details.

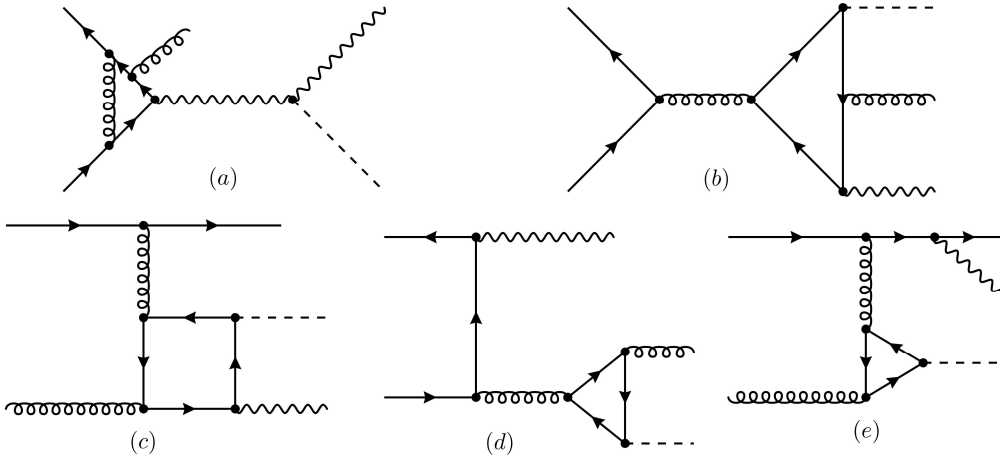


**Figure 1:** Sample Feynman diagrams with quarks or anti-quarks in the initial state. The Drell Yan-type contributions (a) are not included in `ggxy`. Using the switch `iopt_ext_Z` it is possible to include either all contributions from (b)-(e) or only those where both bosons couple to the fermion loop, see (b) and (c).

In addition to the case of stable  $Z$  bosons, we have also implemented the possibility for the  $Z$  boson to decay either into a pair of massless charged leptons ( $Z \rightarrow \ell^- \ell^+$ ) or into a pair of neutrinos ( $Z \rightarrow \nu_\ell \bar{\nu}_\ell$ ), taking into account off-shell effects and spin correlations. The corresponding amplitudes of  $gg \rightarrow \ell\ell H$ , can be constructed by combining the helicity amplitudes of  $gg \rightarrow Z^* H$  and  $Z^* \rightarrow \ell\ell$  as

$$\mathcal{M}(gg \rightarrow \ell\ell H) = \sum_{\lambda} \frac{\mathcal{M}_{\lambda}(gg \rightarrow Z^* H) \mathcal{M}_{\lambda}(Z^* \rightarrow \ell\ell)}{q_Z^2 - m_Z^2 + im_Z \Gamma_Z}, \quad (2.3)$$

where  $q_Z$  is the four momentum of the off-shell  $Z$  boson,  $m_Z$  is the on-shell  $Z$  mass and  $\Gamma_Z$  is the decay width of the  $Z$  boson. The helicity of the  $Z$  boson is indicated by  $\lambda$  while the helicities of all other particles have been suppressed. The maximal value for the off-shellness of the  $Z$  boson is limited in our calculation to about 150 GeV, due to the expansion in the external virtualities of the two-loop amplitudes. Since only the axial-vector coupling of the  $Zt\bar{t}$  vertex contributes to  $gg \rightarrow ZH$ , while the vector component vanishes, the contribution from  $\gamma^* \rightarrow \ell^- \ell^+$  originates only from the real corrections.

For the implementation of the off-shell effects we proceed as follows: In `ggxy` we first evaluate the six form factors numerically, which are used to compute the helicity amplitudes of  $gg \rightarrow Z^* H$ . They are then combined with the helicity amplitudes of the  $Z^*$  decays. The corresponding matrix elements for the real corrections to  $gg \rightarrow \ell\ell H$  can directly be obtained from `Recola`. Note that here, in general, the charged lepton pair can also be produced from an off-shell photon  $\gamma^* \rightarrow \ell^- \ell^+$ .

We have validated the implementation of  $gg \rightarrow ZH$  in `ggxy` in various ways. All partonic routines for the one- and two-loop form factors and for the infra-red subtracted NLO virtual corrections  $\mathcal{V}_{\text{fin}}$  (see Ref. [14] for a precise definition) have been cross-checked against an in-

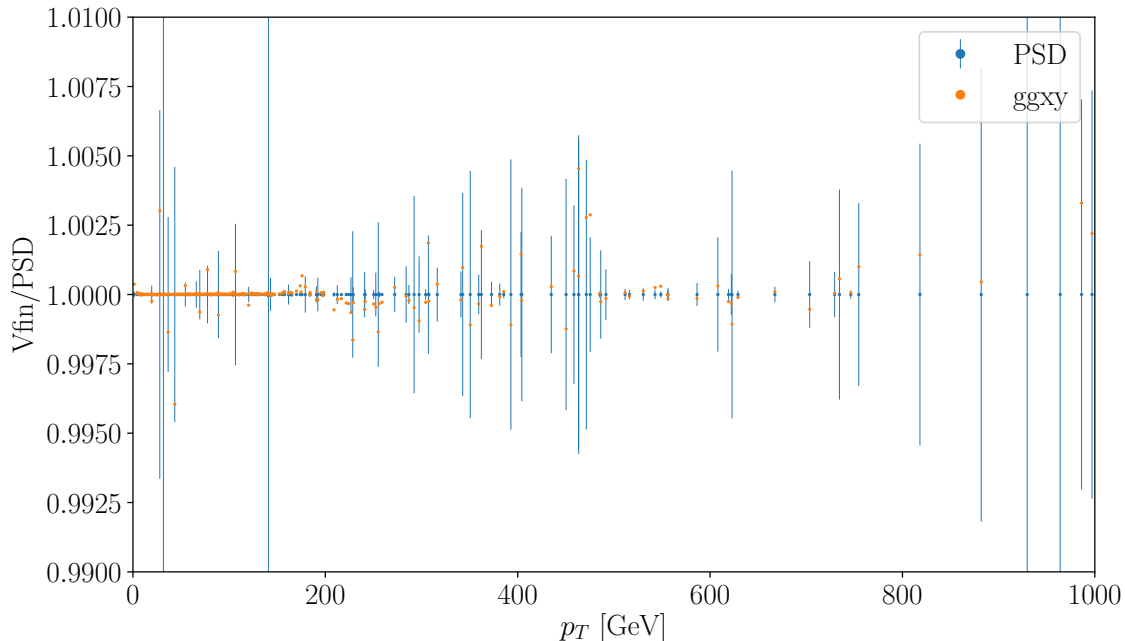


**Figure 2:** Ratio of the finite virtual corrections  $\mathcal{V}_{\text{fin}}$  obtained from `ggxy` and Ref. [12] (“PSD”) as a function of  $p_T$ . The statistical uncertainties of the reference results are shown as well.

house `Mathematica` code, developed in parallel to Ref. [14], which can evaluate using precisions higher than `double`.

In the directory `examples/ggzh-FF/` we provide two examples, `ff.cpp` and `vfin.cpp`, which demonstrate the usage of `ggxy` for the calculation of form factors and  $\mathcal{V}_{\text{fin}}$ . After compilation using `bash build.sh` one can call `run-ff.sh` with the options “1” or “2” to obtain results for fixed values of  $\sqrt{s}$  or and  $p_T$ , respectively. All one- and two-loop form factors are computed for the parameters specified in `run-ff.sh`. The generated data files can be found in the directory `dat/` and all plots for all form factors, separated into real and imaginary parts, can be found in `plots/`. Each plot shows the result from the forward and high-energy expansions and the best approximation as implemented in `ggxy`. The plots for  $F_3^+$  can be compared to Figs. 14 and 15 of Ref. [14].

With the program `vfin.cpp` we demonstrate the functionality and efficiency by performing a comparison of  $\mathcal{V}_{\text{fin}}$  calculated with `ggxy` with the results of Ref. [12] (“PSD”) as shown in Fig. 2. In comparison to Fig. 16 of Ref. [14], we find only minor differences which are due to a different number of expansion terms in the high-energy limit and a different switching point between the forward and high-energy expansions as described above. As a further cross check, we have reproduced the integrated (differential) cross sections of  $gg \rightarrow ZH$  at NLO QCD from Refs. [13, 34]. More details will be provided in the next section.

### 3 Hadronic fixed-order cross sections with ggxy

In this section we describe how `ggxy` can be used to compute hadronic cross sections for  $gg \rightarrow ZH$ . We provide examples where the  $Z$  boson is on-shell and for the production of off-shell  $Z$  bosons which can decay into leptons. The example programs have the same structure as the one for the calculation of NLO QCD corrections to  $gg \rightarrow HH$ , whose implementation is described in detail in Ref. [23]. This concerns, in particular, the information about input parameters such as the choice of the top-quark mass renormalization scheme, the PDF set, or how to define additional histograms. In the following we will concentrate on the parts which are specific to  $gg \rightarrow ZH$ .

#### 3.1 Stable $Z$ bosons

In the example C++ file `examples/ggzh-nlo/nlo-ggzh.cpp` we adapt the input parameters from Ref. [34], which we use throughout the paper if not explicitly stated otherwise. In particular, we use  $m_t = 172.5$  GeV,  $m_Z = 91.1876$  GeV,  $G_F = 1.16637 \cdot 10^{-5}$  GeV<sup>-2</sup> and the PDF4LHC21\_40\_pdfas PDF set [36] via the LHAPDF interface [37]. The renormalization and factorization scales are set to a common scale  $\mu_r = \mu_f = M_{ZH}/2$ , where  $M_{ZH}$  is the invariant mass of the  $ZH$  system.  $Z$  radiation from external quark lines is enabled, and may be controlled in the example program with the variable `iopt_ext_Z = 1` or `iopt_ext_Z = 0`. After compilation (e.g. by executing `bash build.sh`) one can run the example with the help of the script `run.sh` which can be found in the same directory. `bash run.sh 1 1` generates the histogram files in `results-ZH/hist/`. They can be processed with `bash run.sh 2 1` which produces the LO and NLO total cross sections, including the Monte Carlo uncertainty and the uncertainty from the 7-point scale variation at 13.6 TeV. The results are shown in Tab. 1 together with the results from Ref. [34]. For convenience we also show results for  $\sqrt{s} = 13$  TeV and 14 TeV. The comparison of the total cross section to Ref. [13] is shown in Tab. 2, where we adapt the corresponding input values. In both cases `ggxy` is able to reproduce the reference results precisely. The example script demonstrates the cross section computation with different seeds in parallel, where the run-time for each seed is about 90 minutes on a single core, which is three times longer than that of  $gg \rightarrow HH$ . The NLO values in both tables are based on the default setting of five seeds (cores) in parallel.

Running `bash run.sh 2 1` also generates plots for several distributions, which can be found in the directory `results/hist/kfactor/`. In Fig. 3 we show, as examples, the  $ZH$  invariant mass distribution and the transverse momentum distribution of the  $Z$  boson. It is straightforward to adapt the file `examples/ggzh-nlo/nlo-ggzh.cpp` to one's own requirements, see also Ref. [23].

In Fig. 4, we show the comparison with the results from Ref. [34] for the distributions in  $M_{ZH}$  and  $p_{T,Z}$ . The lower panels present the standard deviations with respect to the statistical uncertainties, which shows good agreement between both predictions.

It is possible to change the renormalization between the OS and  $\overline{\text{MS}}$  schemes by setting `scheme` to 0 or 1, respectively. In the latter case one has to provide the renormalization scale

$\sqrt{s}$		ggxy	Ref. [34]
13 TeV	$\sigma^{\text{LO}}$ [fb]	63.97(2) $^{+26.7\%}_{-20.0\%}$	64.0 $^{+27\%}_{-20\%}$
	$\sigma^{\text{NLO}}$ [fb]	118.40(8) $^{+16.5\%}_{-14.0\%}$	118.4 $^{+17\%}_{-14\%}$
13.6 TeV	$\sigma^{\text{LO}}$ [fb]	70.59(2) $^{+26.3\%}_{-19.7\%}$	70.6 $^{+26\%}_{-20\%}$
	$\sigma^{\text{NLO}}$ [fb]	130.50(9) $^{+16.3\%}_{-13.8\%}$	130.5 $^{+16\%}_{-14\%}$
14 TeV	$\sigma^{\text{LO}}$ [fb]	75.15(2) $^{+26.0\%}_{-19.6\%}$	75.2 $^{+26\%}_{-20\%}$
	$\sigma^{\text{NLO}}$ [fb]	139.0(1) $^{+16.3\%}_{-13.7\%}$	138.9 $^{+16\%}_{-14\%}$

**Table 1:** Comparison with results of Ref. [34] at  $\sqrt{s} = \{13, 13.6, 14\}$  TeV.

$\sqrt{s}$		ggxy	Ref. [13]
13 TeV	$\sigma^{\text{LO}}$ [fb]	52.41(2) $^{+25.5\%}_{-19.3\%}$	52.42 $^{+25.5\%}_{-19.3\%}$
	$\sigma^{\text{NLO}}$ [fb]	104.23(6) $^{+16.5\%}_{-13.9\%}$	103.8(3) $^{+16.4\%}_{-13.9\%}$
13.6 TeV	$\sigma^{\text{LO}}$ [fb]	58.06(2) $^{+25.1\%}_{-19.0\%}$	58.06 $^{+25.1\%}_{-19.0\%}$
	$\sigma^{\text{NLO}}$ [fb]	115.16(7) $^{+16.2\%}_{-13.8\%}$	114.7(3) $^{+16.2\%}_{-13.7\%}$
14 TeV	$\sigma^{\text{LO}}$ [fb]	61.95(2) $^{+24.9\%}_{-18.9\%}$	61.96 $^{+24.9\%}_{-18.9\%}$
	$\sigma^{\text{NLO}}$ [fb]	122.64(8) $^{+16.1\%}_{-13.7\%}$	122.2(3) $^{+16.1\%}_{-13.6\%}$

**Table 2:** Comparison with results of Ref. [13] at  $\sqrt{s} = \{13, 13.6, 14\}$  TeV.

of the top quark mass  $\mu_t^2$ , which can either be a fixed or a dynamical scale. In Fig. 5 we show the dependence of the distributions in  $M_{ZH}$  and  $p_{T,H}$  on the choice of top quark mass renormalization scale. We typically observe a downward shift for large invariant mass of the order of 10 – 40%, in line with what has been observed in earlier work on  $gg \rightarrow ZH$  [33]. The variation of the top mass renormalization scheme therefore introduces an uncertainty of a similar size to that of the scale variation of  $\mu_r$  and  $\mu_f$ . In the following we choose to work with the on-shell mass.

### 3.2 Off-shell $Z$ bosons and leptonic decays

An example for the computation of NLO QCD corrections to off-shell  $Z$  production with leptonic decays can be found in the file `examples/ggzh-nlo/nlo-gg1lh.cpp`, where again we adopt the input parameters from Ref. [34]. The final state is controlled by the variable `decaymode` with the values "11" for  $gg \rightarrow \ell^- \ell^+ H$  (default) and "vv" for  $gg \rightarrow \nu_\ell \bar{\nu}_\ell H$ .<sup>2</sup> In addition, the two parameters `mllmin` and `mllmax` control the size of the invariant mass of the

<sup>2</sup>All results calculated with the example program are for a single massless lepton generation, and can be multiplied by 2 to consider also  $\ell = e, \mu$  or 3 for  $\ell = e, \mu, \tau$ .

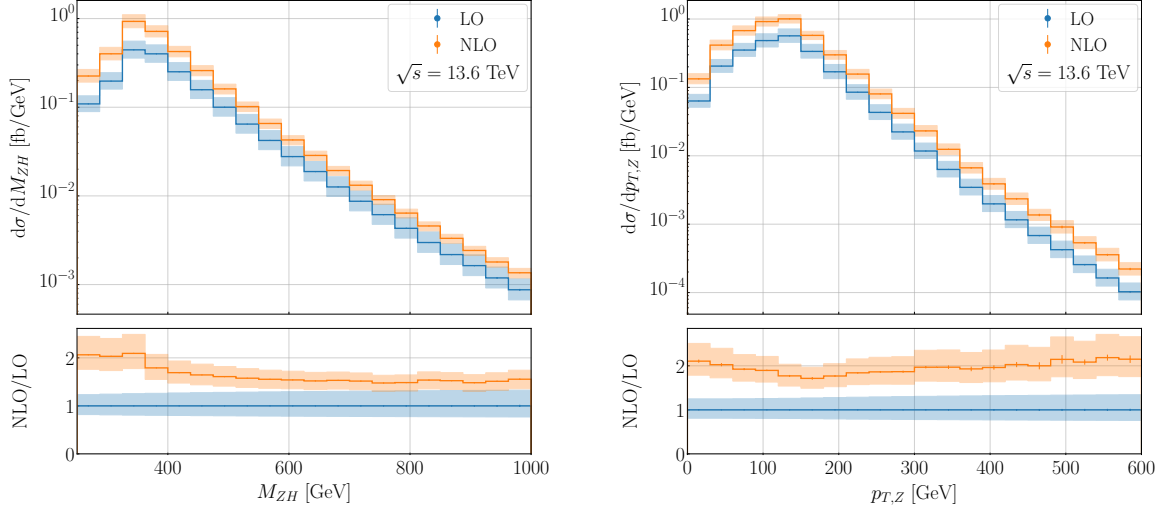


**Figure 3:**  $M_{ZH}$  invariant mass and  $Z$  boson transverse momentum distribution for stable  $Z$  bosons. The input parameters from Ref. [34] have been adapted.

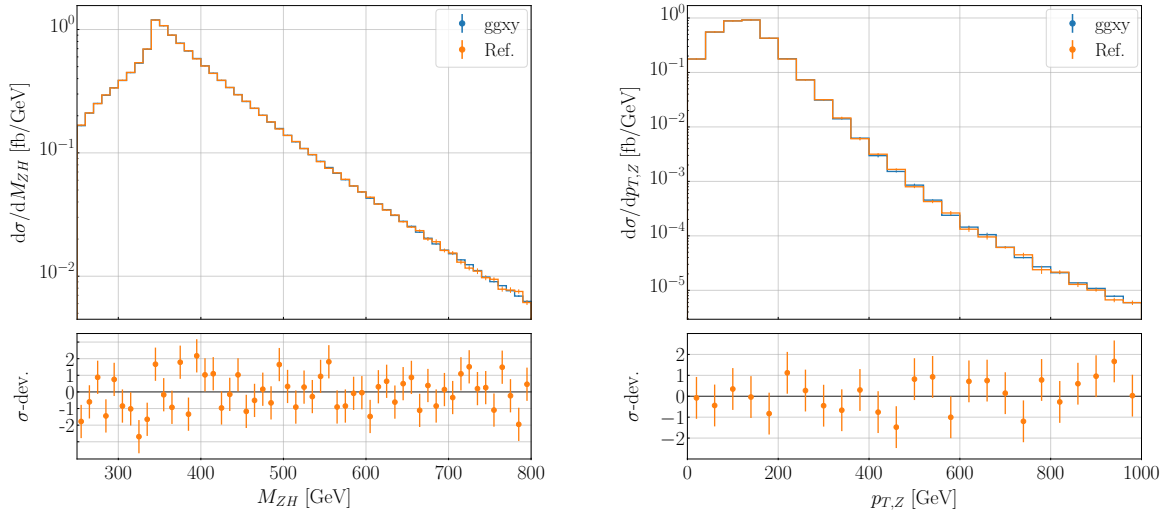


**Figure 4:** Comparison with Ref. [34] for the distributions in  $M_{ZH}$  and  $p_{T,Z}$ . In the lower panels we show the difference of the results normalized to the combined statistical uncertainties.

two-lepton system as  $m_{llmin} < M_{\ell\ell} < m_{llmax}$ . A lower limit is only necessary for  $gg \rightarrow \ell^- \ell^+ H$  since in this case the two charged leptons can be produced from an off-shell photon in the real corrections. We use  $m_{llmin} = 15.0$  (GeV) as the default. The default value of  $m_{llmax}$  is set to 150 GeV and should not be increased due to the expansions in the external virtualities of the virtual amplitudes. Compilation and execution of the sample file proceed as in Section 3.1 where the second input parameter of `run.sh` is “2” instead of “1”. The inclusion of  $Z$  decays

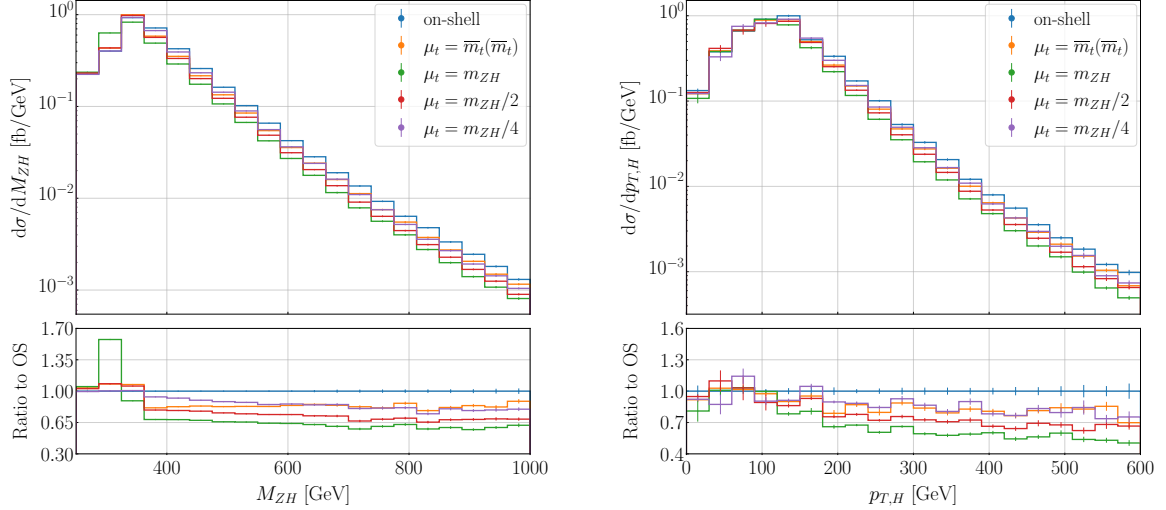


**Figure 5:** Dependence on the top quark mass renormalization scale for the distributions in  $M_{ZH}$  and  $p_{T,H}$ . In the lower panels we show the ratios between the different choices of  $\overline{\text{MS}}$  scales to the on-shell scheme for fixed  $\mu_f = \mu_r = M_{ZH}/2$ .

$\sqrt{s}$		$gg \rightarrow \ell^- \ell^+ H$	$gg \rightarrow \nu_\ell \bar{\nu}_\ell H$
13 TeV	$\sigma^{\text{LO}}$ [fb]	$6.366(4)^{+26.7\%}_{-20.0\%}$	$12.581(8)^{+26.7\%}_{-20.0\%}$
	$\sigma^{\text{NLO}}$ [fb]	$11.80(1)^{+16.6\%}_{-14.0\%}$	$23.30(2)^{+16.5\%}_{-14.0\%}$
13.6 TeV	$\sigma^{\text{LO}}$ [fb]	$7.026(4)^{+26.2\%}_{-19.7\%}$	$13.883(8)^{+26.2\%}_{-19.7\%}$
	$\sigma^{\text{NLO}}$ [fb]	$13.02(1)^{+16.4\%}_{-13.8\%}$	$25.70(2)^{+16.4\%}_{-13.8\%}$
14 TeV	$\sigma^{\text{LO}}$ [fb]	$7.477(5)^{+26.0\%}_{-19.6\%}$	$14.779(9)^{+26.0\%}_{-19.6\%}$
	$\sigma^{\text{NLO}}$ [fb]	$13.84(1)^{+16.3\%}_{-13.8\%}$	$27.30(2)^{+16.3\%}_{-13.7\%}$

**Table 3:** Results for off-shell  $Z$  production with leptonic  $Z$  decays at  $\sqrt{s} = \{13, 13.6, 14\}$  TeV.

has no impact on the runtime.

In Tab. 3 we present results for the integrated cross section for  $gg \rightarrow \ell^- \ell^+ H$  and  $gg \rightarrow \nu_\ell \bar{\nu}_\ell H$  at  $\sqrt{s} = \{13, 13.6, 14\}$  TeV, where in both cases we consider  $\ell = e, \mu, \tau$ . The inclusion of (leptonic)  $Z$  decays has no impact on the size of NLO QCD corrections at the integrated level which are of the order of 85%, as can be seen from the comparison with Tab. 1.

In Fig. 6 we show as an example for the process  $gg \rightarrow \ell^- \ell^+ H$  the  $ZH$  invariant mass and the lepton pair invariant mass. While the former observable is essentially identical to the counterpart shown before for a stable  $Z$  boson, in the latter case the  $Z$  boson peak is clearly visible as well as the enhancement towards small invariant masses  $M_{\ell-\ell^+}$  due to  $\gamma^* \rightarrow \ell^- \ell^+$  starting at NLO. Altogether, after running the example as described

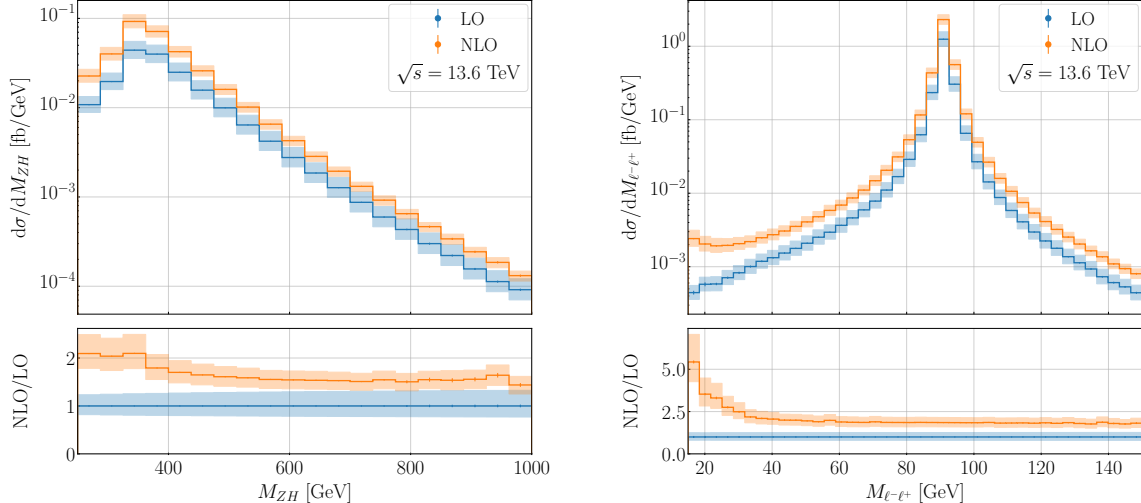


**Figure 6:** LO and NLO QCD predictions for  $M_{ZH}$  and  $M_{\ell^-\ell^+}$  for the  $gg \rightarrow \ell^-\ell^+H$  process.

above, plots for 16 different distributions are generated. They can be found in the directory `examples/ggzh-nlo/results-1lH/kfactor`.

### 3.3 Combination with `vh@nnlo`

Our results for the gluon fusion process can be combined with the Drell-Yan process for  $ZH$ . It starts at LO and is known to N<sup>3</sup>LO [38]; corrections up to NNLO are implemented in the program `vh@nnlo` [19, 20] based on work presented in [3, 5, 39–45]. In the following we use `vh@nnlo` to compute the total cross section.

In Tab. 4 we show the output of `vh@nnlo` for  $\sqrt{s} = 13, 13.6$  and 14 TeV separated into the individual contributions  $\sigma_{\text{top}}$ ,  $\sigma_{\text{DY}}$ ,  $\sigma_{\text{I+II}}$ ,  $\sigma_{b\bar{b} \rightarrow ZH}$ , and  $\sigma_{\text{vh@nnlo}}$ . The first cross section corresponds to the production channel  $gg \rightarrow ZH$ , where the exact leading order is rescaled with the  $K$ -factor obtained from the infinite top mass limit at NLO, the second represents the Drell-Yan like topologies without heavy quark loops, the third to  $q\bar{q}$  induced contributions involving the heavy top quark, and the fourth to  $b\bar{b}$  induced contributions, where the bottom quark is treated as massless, but the Yukawa coupling to the Higgs boson is retained.  $\sigma_{\text{vh@nnlo}} = \sigma_{\text{DY}} + \sigma_{\text{I+II}} + \sigma_{b\bar{b} \rightarrow ZH}$  is the sum of all contributions which are not implemented in `ggxy` and therefore can be safely combined with our implementation of  $gg \rightarrow ZH$ .

In Fig. 7 we show the total  $ZH$  production cross section as a function of the collider energy between 7 and 100 TeV. The dark blue and orange curves correspond to the Drell-Yan contribution at NLO and NNLO, including the uncertainty from the variation of the renormalization and factorization scales, which increases (at NNLO) from 0.5% to 1.5% for higher values of  $\sqrt{s}$ . This is in line with [38] (see also Tab. 4). This contribution does not include the gluon-induced processes, however, it includes the contributions  $\sigma_{\text{I+II}}$  and  $\sigma_{b\bar{b} \rightarrow ZH}$  (see above). For simplicity, we do not consider electroweak corrections since they are implemented in `vh@nnlo` only up to  $\sqrt{s} = 14$  TeV.

$\sqrt{s}$		vh@nnlo
13 TeV	$\sigma_{\text{top}}$ [fb]	122.7(7) $^{+15.6\%}_{-13.6\%}$
	$\sigma_{\text{DY}}$ [fb]	801.9(2) $^{+0.14\%}_{-0.25\%}$
	$\sigma_{\text{I+II}}$ [fb]	11.30(7) $^{+21.9\%}_{-16.9\%}$
	$\sigma_{b\bar{b}\rightarrow ZH}$ [fb]	0.3793(6) $^{+16.3\%}_{-18.5\%}$
	$\sigma_{\text{vh@nnlo}}$ [fb]	813.6(2) $^{+0.32\%}_{-0.49\%}$
13.6 TeV	$\sigma_{\text{top}}$ [fb]	135.3(8) $^{+15.7\%}_{-13.4\%}$
	$\sigma_{\text{DY}}$ [fb]	852.3(2) $^{+0.14\%}_{-0.25\%}$
	$\sigma_{\text{I+II}}$ [fb]	12.01(8) $^{+23.4\%}_{-16.4\%}$
	$\sigma_{b\bar{b}\rightarrow ZH}$ [fb]	0.4218(7) $^{+16.5\%}_{-18.6\%}$
	$\sigma_{\text{vh@nnlo}}$ [fb]	864.7(2) $^{+0.34\%}_{-0.48\%}$
14 TeV	$\sigma_{\text{top}}$ [fb]	144.0(8) $^{+15.7\%}_{-13.4\%}$
	$\sigma_{\text{DY}}$ [fb]	886.2(2) $^{+0.14\%}_{-0.25\%}$
	$\sigma_{\text{I+II}}$ [fb]	12.62(9) $^{+22.9\%}_{-17.1\%}$
	$\sigma_{b\bar{b}\rightarrow ZH}$ [fb]	0.4513(7) $^{+16.6\%}_{-18.7\%}$
	$\sigma_{\text{vh@nnlo}}$ [fb]	899.2(3) $^{+0.34\%}_{-0.49\%}$

**Table 4:** Results for vh@nnlo at  $\sqrt{s} = \{13, 13.6, 14\}$  TeV.  $\sigma_{\text{top}}$  is the reweighted  $gg \rightarrow ZH$  contributions, which we replace with our calculation. The Drell-Yan like contributions are given by  $\sigma_{\text{DY}}$ . Top quark effects in the Drell-Yan like contributions are given by  $\sigma_{\text{I+II}}$ . Bottom quark induced processes are given by  $\sigma_{b\bar{b}\rightarrow ZH}$ . We define  $\sigma_{\text{vh@nnlo}} = \sigma_{\text{DY}} + \sigma_{\text{I+II}} + \sigma_{b\bar{b}\rightarrow ZH}$  as the contributions to which we want to add to our new predictions, i.e. omitting  $\sigma_{\text{top}}$ .

The green and red bands in Fig. 7 show the total cross section including the gluon-induced channel, where the green band only includes LO result and the red also the NLO corrections. The size of the gluon-fusion contribution increases from 5% to 25% of the DY contribution for rising values of  $\sqrt{s}$ . The NLO cross section is about twice the size. At LHC energies we observe a 15% effect of the  $gg$  channel. By including the NLO corrections, the scale uncertainties from the gluon-fusion contribution decrease from 22% – 33% to 19% – 13%, where the scale uncertainties decreases towards higher values of  $\sqrt{s}$ . The inclusion of the  $gg$  channel in  $ZH$  production increases the combined scale uncertainties to 2% – 5%.

For the  $gg \rightarrow ZH$  channel, we also show the NLO corrections as obtained from the rescaling of the exact LO result with the  $K$  factor obtained from the NLO heavy-top contribution, in the light-blue curve. We observe that the deviation from the exact NLO result is between 1% – 2% over the whole energy range. Differential distributions usually show larger deviations from the naive heavy top quark limit, see for example the discussion for the similar  $gg \rightarrow HH$  process in Ref. [46]. The NLO corrections are large and need to be taken into account.

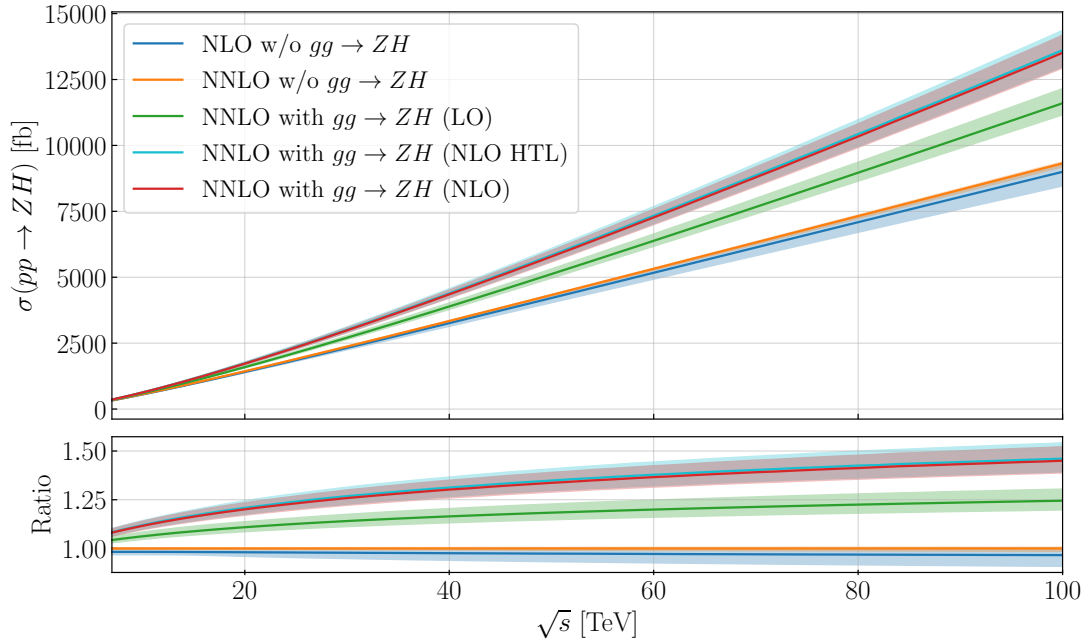


**Figure 7:** Total cross section for  $ZH$  production as a function of the collider energy up to  $\sqrt{s} = 100$  TeV. We separately show the cross section at NLO and NNLO without the gluon-induced channel and at NNLO including LO and also NLO contributions from  $gg \rightarrow ZH$ .

In Ref. [38] the N3LO DY contributions have been calculated, and amount to about 1% – 2%, while the scale uncertainties barely change. Since for the total cross section the scale uncertainties are dominated by the  $gg \rightarrow ZH$  process and the rescaling by the heavy top quark mass limit delivers reliable results at NLO, this motivates the full calculation of NNLO corrections to  $gg \rightarrow ZH$  in this limit. The virtual corrections are already known and are given in Ref. [15].

## 4 $gg \rightarrow ZH$ at NLO matched to a parton shower

### 4.1 Implementation in POWHEG: ggxy\_ggZH

In the following we describe the new implementation of  $gg \rightarrow ZH$ , including NLO QCD corrections, in POWHEG [47] via an interface to ggxy, which allows the combination with parton showers from e.g. Pythia [24] or Herwig [48]. We note that this interface is based on the POWHEG process implementation of  $gg \rightarrow HH$ .<sup>3</sup> For  $gg \rightarrow ZH$  we consider a leptonically-decaying  $Z$  boson, into either a charged lepton or neutrino pair, taking into account spin correlations as well as off-shell effects at the matrix element level. This code can be obtained from [https://gitlab.com/POWHEG-BOX/V2/User-Processes/ggxy\\_ggZH](https://gitlab.com/POWHEG-BOX/V2/User-Processes/ggxy_ggZH).

<sup>3</sup>[https://gitlab.com/POWHEG-BOX/V2/User-Processes/ggxy\\_ggHH](https://gitlab.com/POWHEG-BOX/V2/User-Processes/ggxy_ggHH)

In an alternative approach (primarily for testing purposes) we have also implemented  $gg \rightarrow ZH$  with a stable  $Z$  boson.<sup>4</sup> In this case, the  $Z$  decays can be generated with the parton shower Monte Carlo program. Differences of both implementations at the differential level will be discussed in Section 4.3.

All one-loop matrix elements are calculated with `Recola`, while the virtual corrections are obtained from `ggxy`. It is thus necessary first to install `ggxy` and to define the path to the directory `example-install` of `ggxy` in the variable `path_to_ggxy` in the file `env-vars.sh`, which can be found in the `POWHEG` directory. The `POWHEG` process can then be compiled with `source env-vars.sh` followed by `make`, for more details see also the `README.md` of the process implementation.

This implementation is as flexible as the one which only uses `ggxy`, see the previous sections, and allows for the variation of all input parameters as well as the top-quark mass renormalization scheme. The invariant mass range of the two lepton/neutrino system can be specified with the variables `min_z_mass` and `max_z_mass`, where the default values are set to 15 GeV and 150 GeV, respectively. Smaller values of `min_z_mass` might lead to a less efficient event generation, and the value of `max_z_mass` should not be increased as the two-loop amplitudes are expansions in the virtualities of the (off-shell)  $Z$  and Higgs bosons. To improve the numerical stability, we have implemented a technical cut where we discard events in the real corrections that contain a radiated parton with a transverse momentum of less than 0.1 GeV, see also Ref. [49]. Further information about process-dependent parameters of the `POWHEG` implementation can be found in the `README.md` file.

After installation, an example setup can be found in the directory `testrun`, which can be started with `run.sh`. Input parameters should be adjusted beforehand in the file `powheg.input-save`. The script `run.sh` runs through all four stages of `POWHEG`, where the first stage is used to optimize the phase-space generation. Differential distributions and the total cross section are calculated in the second stage. The output of stage two represents the fixed-order results and can be directly compared with the output of `ggxy`. Stage 3 is used to initialize the event generation that is carried out in stage 4.

## 4.2 Cross checks with `ggxy`

We have performed several cross checks of the fixed-order results from `POWHEG` after the end of stage 2 with the results from `ggxy`. For stable  $Z$  bosons we reproduce the integrated cross section at  $\sqrt{s} = 13.6$  TeV from Tab. 1 and obtain

$$\begin{aligned}\sigma_{gg \rightarrow ZH}^{\text{NLO}}(\text{ggxy}) &= 130.50(9) \text{ fb}, \\ \sigma_{gg \rightarrow ZH}^{\text{NLO}}(\text{POWHEG}) &= 130.56(4) \text{ fb},\end{aligned}$$

where we find an agreement between the two calculation within less than one standard deviation. In addition, we have also cross-checked the two implementations at the differential level. As

---

<sup>4</sup>This implementation can be download from [https://gitlab.com/ggxy/ggxy\\_ggZH-stable](https://gitlab.com/ggxy/ggxy_ggZH-stable).

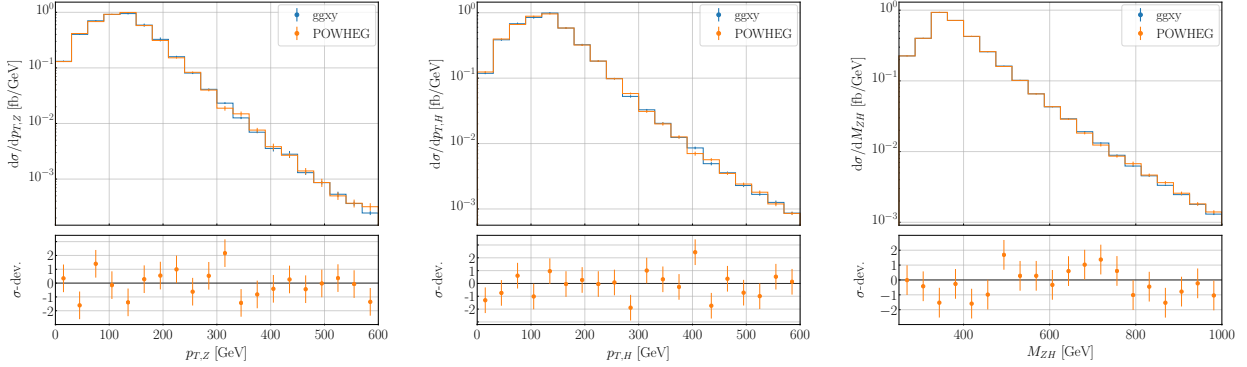


**Figure 8:** Differential distributions for the observables  $p_{T,Z}$ ,  $p_{T,H}$  and  $M_{ZH}$  at NLO QCD for the  $gg \rightarrow ZH$  process at  $\sqrt{s} = 13.6$  TeV computed with `ggxy` and the `POWHEG` interface. In the lower panels we show the difference of the results normalized to the combined statistical uncertainties.

possible examples, we show in Fig. 8 the transverse momentum of the  $Z$  and Higgs bosons as well as the invariant mass of the  $ZH$  system. Overall the calculations agree very well.

We have performed similar cross-checks for the  $gg \rightarrow \ell^- \ell^+ H$  process. Also in this case we reproduce the results at the level of the integrated cross section from the computation with `ggxy` from Tab. 3:

$$\begin{aligned} \sigma_{gg \rightarrow \ell^- \ell^+ H}^{\text{NLO}}(\text{ggxy}) &= 13.02(1) \text{ fb}, \\ \sigma_{gg \rightarrow \ell^- \ell^+ H}^{\text{NLO}}(\text{POWHEG}) &= 13.01(1) \text{ fb}. \end{aligned}$$

Similarly good agreement is also found at the differential level. In Fig. 9 we present, as an example, the differential cross sections w.r.t. the invariant mass of the lepton pair,  $M_{\ell^- \ell^+}$ , the rapidity of the positively charged lepton  $y_{\ell^+}$  and its transverse momentum  $p_{T,\ell^-}$ . In all cases we find good agreement between both calculations.

### 4.3 Numerical results for parton showers with Pythia

In this section we discuss parton shower effects and the modeling of the  $Z$ -boson decays at the differential level. For clarity, we consider the process the  $gg \rightarrow e^- e^+ H$ . We use the parton shower of `Pythia 8.2` [24]; an example program (`main-PYTHIA8.f`) can be found in the corresponding `POWHEG` implementation as well as an example run in the directory `test-pythia8`. We use as default the same value for `hdamp = 250` in `POWHEG` as for the calculation of  $gg \rightarrow HH$  presented in Ref. [50]. This parameter can be used to divide the real corrections into two separate contributions  $R = R_s + R_f$  with

$$R_s = F_{\text{damp}} R, \quad R_f = (1 - F_{\text{damp}}) R, \quad (4.1)$$

with

$$F_{\text{damp}} = \frac{h_{\text{damp}}^2}{h_{\text{damp}}^2 + k_T^2}, \quad (4.2)$$

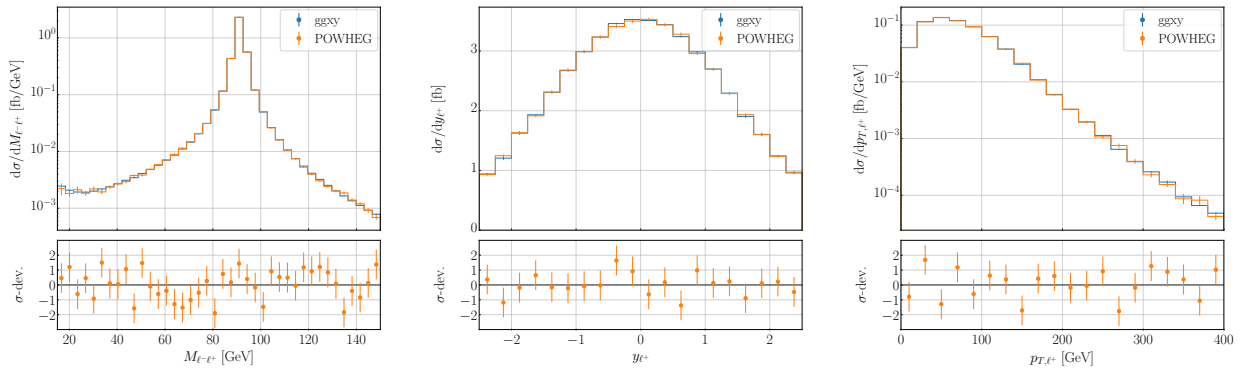


**Figure 9:** Differential distributions in the observables  $M_{\ell-\ell^+}$ ,  $y_{\ell^+}$  and  $p_{T,\ell^+}$  at NLO QCD for the  $gg \rightarrow \ell^-\ell^+H$  process at  $\sqrt{s} = 13.6$  TeV computed with `ggxy` and the `POWHEG` interface. In the lower panels we show the difference of the results normalized to the combined statistical uncertainties.

where  $k_T^2$  is the transverse momentum of the radiation. The singular contribution  $R_s$  is used in the matching procedure, while the finite contribution  $R_f$  is treated as in a regular fixed-order calculation. The `POWHEG` default value corresponds to `hdamp` =  $\infty$ , i.e.,  $F_{\text{damp}} = 1$ . Changing this value corresponds to tuning the real cross section such that it follows the fixed-order results at large transverse momenta more closely, which becomes especially relevant in the case of large corrections from real radiation. Differences between the two choices will be discussed later in this section.

In Fig. 10 we compare the fixed-order predictions of the  $gg \rightarrow e^-e^+H$  process at NLO QCD computed with `ggxy` (NLO) with two different predictions including parton shower effects. The two predictions matched to the parton shower of `Pythia` only differ in the modeling of the  $Z$  boson, where the predictions labeled with “NLO+PS” contain, as the fixed-order results, the  $Z$  boson decays already at the matrix element retaining all off-shell effects and spin correlations. The second prediction containing parton shower effects, “NLO+PS-stable”, is generated with our second implementation for a stable  $Z$  boson in `POWHEG`, where the  $Z$  boson decays are simulated with `Pythia`.

We find that, in general, the naive approach without spin correlations fails to precisely describe angular distributions of the two leptons such as the azimuthal angle between the electron-positron pair,  $\Delta\phi_{e^-e^+}$ , or the transverse momentum distribution of the positron  $p_{T,e^+}$ . The differences range from 40% – 100% and are significantly larger than the scale uncertainties of the fixed-order calculation. On the other hand, the numerical results for the rapidity of the positron  $y_{e^+}$  are essentially the same for all three approaches. This is the only leptonic observable for which we found that the inclusion of spin correlations is irrelevant. Also for observables that are built from the reconstructed  $Z$  boson, the inclusion of spin correlations does not lead to any improvement as can be seen, e.g., from the invariant mass of the  $ZH$  system  $M_{ZH}$ . Out of these four observables we find only for  $p_{T,e^+}$  sizable parton shower effects, which increase towards the tails to more than 20% and become similar in size to the corresponding

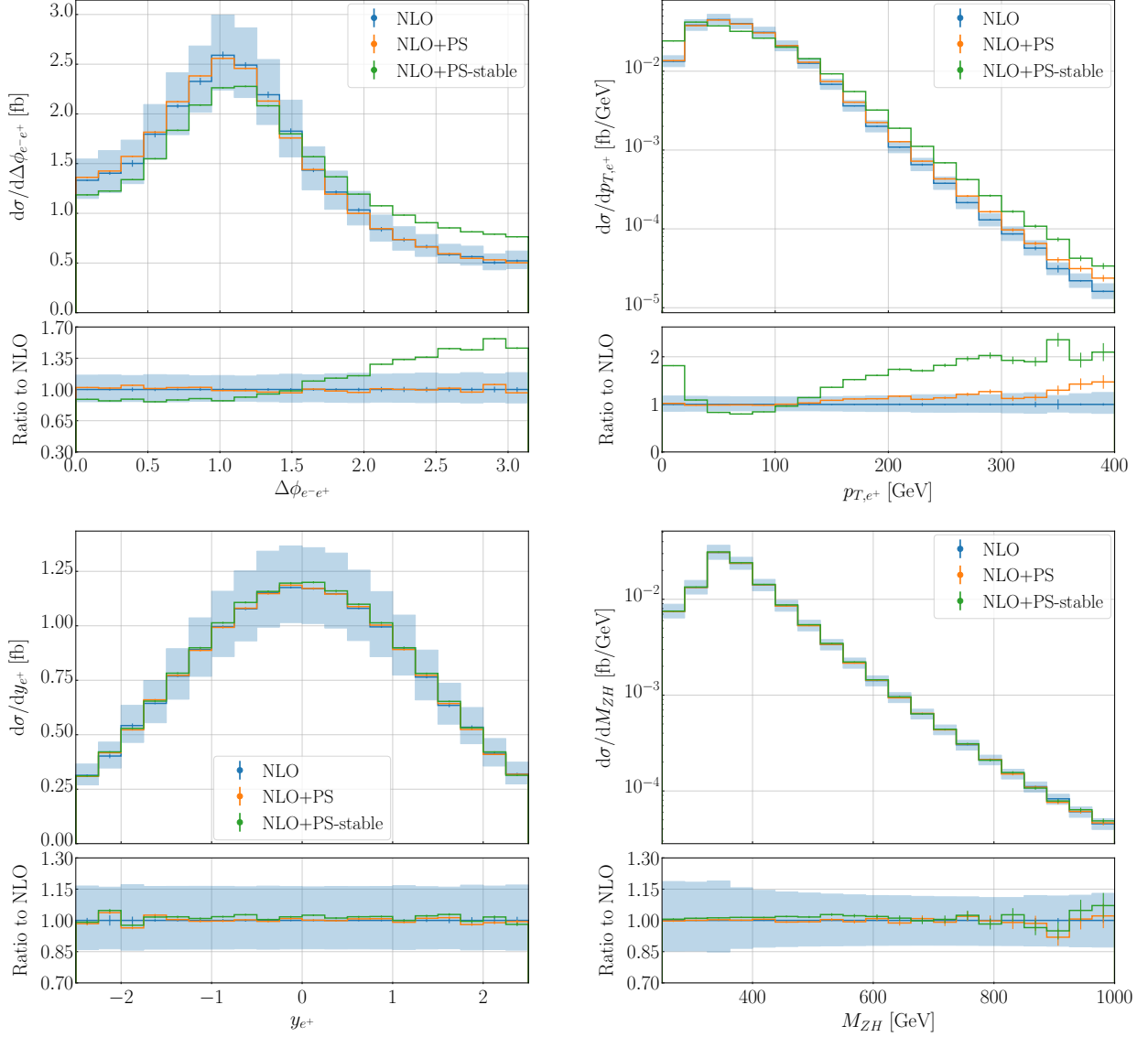


**Figure 10:** Differential distributions for the observables  $\Delta\phi_{e^-e^+}$ ,  $p_{T,e^+}$ ,  $y_{e^+}$  and  $M_{ZH}$  for the  $gg \rightarrow e^-e^+H$  process at NLO QCD. Results are shown at fixed-order (NLO), including parton shower effects with (NLO+PS) and without (NLO+PS-stable)  $Z$  boson decays at the matrix element level.

scale uncertainties of the fixed-order calculation.

In Fig. 11 we show the differential distributions of  $p_{T,ZH}$  and  $p_{T,H}$  for the  $gg \rightarrow e^-e^+H$  at fixed-order as well as two results matched to parton showers, where we use for the POWHEG input parameter  $h_{\text{damp}} = 250$  and  $h_{\text{damp}} = \infty$ . These two observables have rather large parton shower effects compared to the rest that we have considered. For  $p_{T,ZH}$  it is fairly clear that the inclusion of parton shower effects lead to significant shape changes, as at fixed-order (NLO) we have  $p_{T,ZH} = p_{T,j}$ , where  $j$  is the additional radiation in the real corrections. We observe that the additional radiation from the parton shower leads to a softer distribution at small  $p_{T,ZH}$

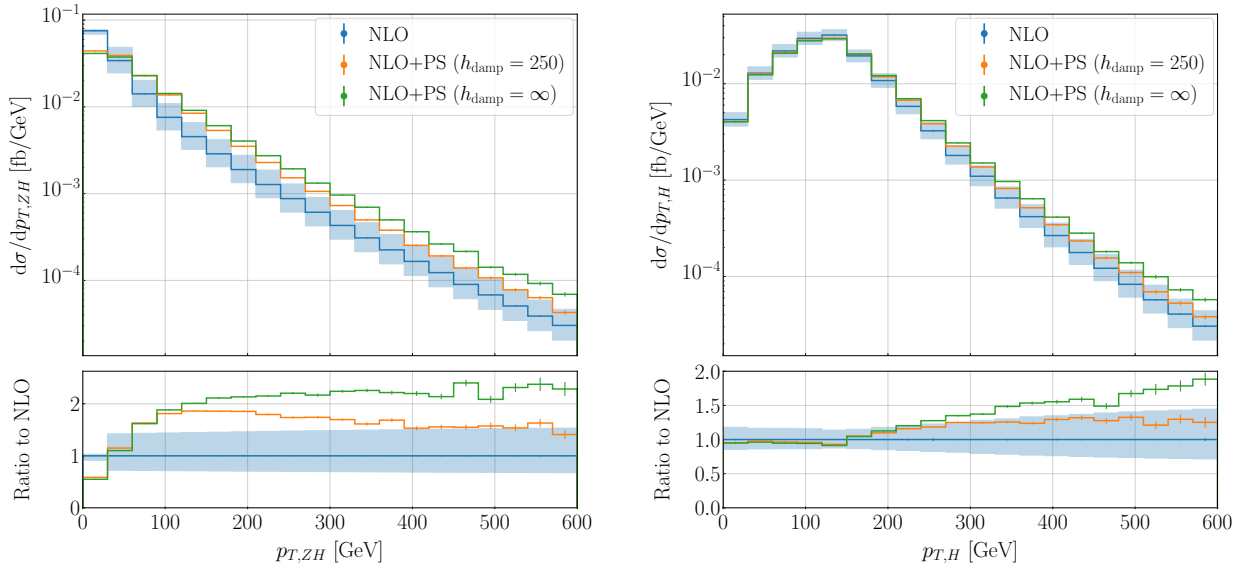


**Figure 11:** Differential distributions for the observables  $p_{T,ZH}$  and  $p_{T,H}$  for the  $gg \rightarrow e^- e^+ H$  process at NLO QCD. Results are shown at fixed-order and including parton shower effects with  $h_{\text{damp}} = 250$  and  $h_{\text{damp}} = \infty$ .

and to a harder spectrum in the tail, with differences up to 100% for  $h_{\text{damp}} = \infty$  with respect to the fixed-order prediction.

For  $p_{T,H}$  we find that the inclusion of parton shower effects leads to an increase of more than 80% in the tail. One reason for such large effects is the size of the NLO corrections in this region, which are as large as 700% (not shown in the panel), due to the inclusion of diagrams with  $Z$  radiation off external quark lines in real corrections. For both distributions it is possible to choose a different value from  $h_{\text{damp}} = \infty$  such that the tails of the parton shower predictions are closer to the ones of the fixed-order results. With  $h_{\text{damp}} = 250$  the size of the parton shower effects for both observables decrease by half to about 40% – 50%.

## 5 Conclusions

In this paper we describe the implementation of NLO QCD corrections to  $gg \rightarrow ZH$  in the **C++** library **gqxy**. It is based on deep expansions in the large- $m_t$  limit, around the forward limit and for high energies. **gqxy** provides a framework which allows for a flexible choice of all input parameters. For the renormalization scheme of the top quark mass one can either choose the on-shell or the  $\overline{\text{MS}}$  scheme with arbitrary renormalization scale  $\mu_t$ . Furthermore, it is possible to consider either stable  $Z$  bosons or their leptonic decays into charged leptons or neutrinos at the amplitude level.

We provide an interface to **POWHEG** which we use for the matching to parton showers. The latter are realized with the help of **Pythia**. This allows us to compare the effect of  $Z$  boson decays at the level of the amplitude to decays generated during the showering process.

The latest version of `ggxy` can be downloaded from <https://gitlab.com/ggxy/ggxy-release> and the POWHEG implementation from [https://gitlab.com/POWHEG-BOX/V2/User-Processes/ggxy\\_ggZH](https://gitlab.com/POWHEG-BOX/V2/User-Processes/ggxy_ggZH).

## Acknowledgements

This work was supported by the Deutsche Forschungsgemeinschaft (DFG, German Research Foundation) under grant 396021762 — TRR 257 “Particle Physics Phenomenology after the Higgs Discovery”. The work of J.D. was supported by STFC Consolidated Grant ST/X000699/1. K.S. is supported by the European Union under the Marie Skłodowska-Curie Actions (MSCA) Grant 101204018. We thank Benjamin Campillo for providing results for the real corrections for individual phase-space points and for providing the data points for the observables shown in Fig. 4.

## References

- [1] ATLAS collaboration, *Measurements of  $WH$  and  $ZH$  production with Higgs boson decays into bottom quarks and direct constraints on the charm Yukawa coupling in 13 TeV  $pp$  collisions with the ATLAS detector*, *JHEP* **04** (2025) 075 [[2410.19611](#)].
- [2] CMS collaboration, *Measurement of simplified template cross sections of the Higgs boson produced in association with  $W$  or  $Z$  bosons in the  $H \rightarrow bb^-$  decay channel in proton-proton collisions at  $s=13$  TeV*, *Phys. Rev. D* **109** (2024) 092011 [[2312.07562](#)].
- [3] B. A. Kniehl, *Associated Production of Higgs and  $Z$  Bosons From Gluon Fusion in Hadron Collisions*, *Phys. Rev. D* **42** (1990) 2253.
- [4] D. A. Dicus and C. Kao, *Higgs Boson -  $Z^0$  Production From Gluon Fusion*, *Phys. Rev. D* **38** (1988) 1008.
- [5] M. L. Ciccolini, S. Dittmaier and M. Kramer, *Electroweak radiative corrections to associated  $WH$  and  $ZH$  production at hadron colliders*, *Phys. Rev. D* **68** (2003) 073003 [[hep-ph/0306234](#)].
- [6] G. Ferrera, M. Grazzini and F. Tramontano, *Associated  $ZH$  production at hadron colliders: the fully differential NNLO QCD calculation*, *Phys. Lett. B* **740** (2015) 51 [[1407.4747](#)].
- [7] J. M. Campbell, R. K. Ellis and C. Williams, *Associated production of a Higgs boson at NNLO*, *JHEP* **06** (2016) 179 [[1601.00658](#)].
- [8] A. Hasselhuhn, T. Luthe and M. Steinhauser, *On top quark mass effects to  $gg \rightarrow ZH$  at NLO*, *JHEP* **01** (2017) 073 [[1611.05881](#)].
- [9] J. Davies, G. Mishima and M. Steinhauser, *Virtual corrections to  $gg \rightarrow ZH$  in the high-energy and large- $m_t$  limits*, *JHEP* **03** (2021) 034 [[2011.12314](#)].
- [10] G. Wang, X. Xu, Y. Xu and L. L. Yang, *Next-to-leading order corrections for  $gg \rightarrow ZH$  with top quark mass dependence*, *Phys. Lett. B* **829** (2022) 137087 [[2107.08206](#)].
- [11] L. Alasfar, G. Degrossi, P. P. Giardino, R. Gröber and M. Vitti, *Virtual corrections to  $gg \rightarrow ZH$  via a transverse momentum expansion*, *JHEP* **05** (2021) 168 [[2103.06225](#)].

- [12] L. Chen, G. Heinrich, S. P. Jones, M. Kerner, J. Klappert and J. Schlenk, *ZH production in gluon fusion: two-loop amplitudes with full top quark mass dependence*, *JHEP* **03** (2021) 125 [[2011.12325](#)].
- [13] L. Chen, J. Davies, G. Heinrich, S. P. Jones, M. Kerner, G. Mishima et al., *ZH production in gluon fusion at NLO in QCD*, *JHEP* **08** (2022) 056 [[2204.05225](#)].
- [14] J. Davies, D. Grau, K. Schönwald, M. Steinhauser, D. Stremmer and M. Vitti, *Two-loop QCD corrections to ZH and off-shell Z boson pair production in gluon fusion*, [2509.07072](#).
- [15] J. Davies, D. Grau, K. Schönwald, M. Steinhauser and D. Stremmer, *Three-loop corrections to  $gg \rightarrow ZH$  in the large top quark mass limit*, [2512.00156](#).
- [16] M. C. Kumar, M. K. Mandal and V. Ravindran, *Associated production of Higgs boson with vector boson at threshold  $N^3LO$  in QCD*, *JHEP* **03** (2015) 037 [[1412.3357](#)].
- [17] R. V. Harlander, A. Kulesza, V. Theeuwes and T. Zirke, *Soft gluon resummation for gluon-induced Higgs Strahlung*, *JHEP* **11** (2014) 082 [[1410.0217](#)].
- [18] G. Das, C. Dey, M. C. Kumar and K. Samanta, *Soft gluon resummation for gluon fusion ZH production*, *Phys. Rev. D* **113** (2026) 014024 [[2501.10330](#)].
- [19] O. Brein, R. V. Harlander and T. J. E. Zirke, *vh@nnlo - Higgs Strahlung at hadron colliders*, *Comput. Phys. Commun.* **184** (2013) 998 [[1210.5347](#)].
- [20] R. V. Harlander, J. Klappert, S. Liebler and L. Simon, *vh@nnlo-v2: New physics in Higgs Strahlung*, *JHEP* **05** (2018) 089 [[1802.04817](#)].
- [21] A. Denner, S. Dittmaier, S. Kallweit and A. Muck, *Electroweak corrections to Higgs-strahlung off W/Z bosons at the Tevatron and the LHC with HAWK*, *JHEP* **03** (2012) 075 [[1112.5142](#)].
- [22] A. Denner, S. Dittmaier, S. Kallweit and A. Mück, *HAWK 2.0: A Monte Carlo program for Higgs production in vector-boson fusion and Higgs strahlung at hadron colliders*, *Comput. Phys. Commun.* **195** (2015) 161 [[1412.5390](#)].
- [23] J. Davies, K. Schönwald, M. Steinhauser and D. Stremmer, *ggxy: A flexible library to compute gluon-induced cross sections*, *Comput. Phys. Commun.* **320** (2026) 109933 [[2506.04323](#)].
- [24] T. Sjostrand, S. Mrenna and P. Z. Skands, *A Brief Introduction to PYTHIA 8.1*, *Comput. Phys. Commun.* **178** (2008) 852 [[0710.3820](#)].
- [25] J. Davies, G. Mishima, M. Steinhauser and D. Wellmann,  *$gg \rightarrow ZZ$ : analytic two-loop results for the low- and high-energy regions*, *JHEP* **04** (2020) 024 [[2002.05558](#)].
- [26] A. van Hameren, *OneLOop: For the evaluation of one-loop scalar functions*, *Comput. Phys. Commun.* **182** (2011) 2427 [[1007.4716](#)].
- [27] S. Catani and M. H. Seymour, *A General algorithm for calculating jet cross-sections in NLO QCD*, *Nucl. Phys. B* **485** (1997) 291 [[hep-ph/9605323](#)].
- [28] S. Actis, A. Denner, L. Hofer, A. Scharf and S. Uccirati, *Recursive generation of one-loop amplitudes in the Standard Model*, *JHEP* **04** (2013) 037 [[1211.6316](#)].
- [29] S. Actis, A. Denner, L. Hofer, J.-N. Lang, A. Scharf and S. Uccirati, *RECOLA: REcursive Computation of One-Loop Amplitudes*, *Comput. Phys. Commun.* **214** (2017) 140 [[1605.01090](#)].

- [30] A. Denner, S. Dittmaier and L. Hofer, *Collier: a fortran-based Complex One-Loop Library in Extended Regularizations*, *Comput. Phys. Commun.* **212** (2017) 220 [[1604.06792](#)].
- [31] G. Ossola, C. G. Papadopoulos and R. Pittau, *Reducing full one-loop amplitudes to scalar integrals at the integrand level*, *Nucl. Phys. B* **763** (2007) 147 [[hep-ph/0609007](#)].
- [32] G. Ossola, C. G. Papadopoulos and R. Pittau, *CutTools: A Program implementing the OPP reduction method to compute one-loop amplitudes*, *JHEP* **03** (2008) 042 [[0711.3596](#)].
- [33] G. Degrossi, R. Gröber, M. Vitti and X. Zhao, *On the NLO QCD corrections to gluon-initiated ZH production*, *JHEP* **08** (2022) 009 [[2205.02769](#)].
- [34] B. Campillo Aveleira et al., *gg → ZH : updated predictions at NLO QCD*, 8, 2025, [2508.09905](#).
- [35] F. A. Berends and W. T. Giele, *Recursive Calculations for Processes with n Gluons*, *Nucl. Phys. B* **306** (1988) 759.
- [36] PDF4LHC WORKING GROUP collaboration, *The PDF4LHC21 combination of global PDF fits for the LHC Run III*, *J. Phys. G* **49** (2022) 080501 [[2203.05506](#)].
- [37] A. Buckley, J. Ferrando, S. Lloyd, K. Nordström, B. Page, M. Rüfenacht et al., *LHAPDF6: parton density access in the LHC precision era*, *Eur. Phys. J. C* **75** (2015) 132 [[1412.7420](#)].
- [38] J. Baglio, C. Duhr, B. Mistlberger and R. Szafron, *Inclusive production cross sections at N<sup>3</sup>LO*, *JHEP* **12** (2022) 066 [[2209.06138](#)].
- [39] T. Han and S. Willenbrock, *QCD correction to the p p → WH and ZH total cross-sections*, *Phys. Lett. B* **273** (1991) 167.
- [40] R. Hamberg, W. L. van Neerven and T. Matsuura, *A complete calculation of the order α – s<sup>2</sup> correction to the Drell-Yan K factor*, *Nucl. Phys. B* **359** (1991) 343.
- [41] R. V. Harlander and W. B. Kilgore, *Next-to-next-to-leading order Higgs production at hadron colliders*, *Phys. Rev. Lett.* **88** (2002) 201801 [[hep-ph/0201206](#)].
- [42] O. Brein, A. Djouadi and R. Harlander, *NNLO QCD corrections to the Higgs-strahlung processes at hadron colliders*, *Phys. Lett. B* **579** (2004) 149 [[hep-ph/0307206](#)].
- [43] O. Brein, R. Harlander, M. Wiesemann and T. Zirke, *Top-Quark Mediated Effects in Hadronic Higgs-Strahlung*, *Eur. Phys. J. C* **72** (2012) 1868 [[1111.0761](#)].
- [44] L. Altenkamp, S. Dittmaier, R. V. Harlander, H. Rzehak and T. J. E. Zirke, *Gluon-induced Higgs-strahlung at next-to-leading order QCD*, *JHEP* **02** (2013) 078 [[1211.5015](#)].
- [45] R. V. Harlander, S. Liebler and T. Zirke, *Higgs Strahlung at the Large Hadron Collider in the 2-Higgs-Doublet Model*, *JHEP* **02** (2014) 023 [[1307.8122](#)].
- [46] S. Borowka, N. Greiner, G. Heinrich, S. P. Jones, M. Kerner, J. Schlenk et al., *Full top quark mass dependence in Higgs boson pair production at NLO*, *JHEP* **10** (2016) 107 [[1608.04798](#)].
- [47] S. Alioli, P. Nason, C. Oleari and E. Re, *A general framework for implementing NLO calculations in shower Monte Carlo programs: the POWHEG BOX*, *JHEP* **06** (2010) 043 [[1002.2581](#)].
- [48] J. Bellm et al., *The Physics of Herwig 7*, [2512.16645](#).

- [49] S. Alioli, S. Ferrario Ravasio, J. M. Lindert and R. Röntsch, *Four-lepton production in gluon fusion at NLO matched to parton showers*, *Eur. Phys. J. C* **81** (2021) 687 [[2102.07783](#)].
- [50] G. Heinrich, S. P. Jones, M. Kerner, G. Luisoni and E. Vryonidou, *NLO predictions for Higgs boson pair production with full top quark mass dependence matched to parton showers*, *JHEP* **08** (2017) 088 [[1703.09252](#)].